JOURNAL OF GEOPHYSICAL RESEARCH, VOL. 101, NO. B8, PAGES 17,535–17,545, AUGUST 10, 1996

Sound velocity and elasticity of single-crystal forsterite to 16 GPa

Chang-Sheng Zha, Thomas S. Duffy,[1] Robert T. Downs, Ho-Kwang Mao, and Russell J. Hemley

Geophysical Laboratory and Center for High-Pressure Research, Carnegie Institution of Washington, D. C.

Abstract. As an abundant component of Earth's upper mantle, forsterite (Mg_2SiO_4) has been the subject of extensive investigation for many decades. The pressure dependences of sound velocity and elasticity are of great importance for modeling the composition and evolution of Earth. For this reason, room temperature Brillouin scattering experiments were performed on single-crystal forsterite at pressures up to 16 GPa in a diamond anvil cell. The nine elastic moduli increase linearly over the pressure range studied. Together with previous ambient pressure data, the pressure variation of the bulk modulus is K_S(GPa) = 128.8(5) + 4.2(2)P, and the shear modulus is G(GPa) = 81.6(2) + 1.4(1)P, where the numbers in parentheses are one standard deviation uncertainties in the last digit. Combining with previous ultrasonic data for polycrystalline β-Mg_2SiO_4 to 3 GPa, the sound velocity contrasts between α- and β-Mg_2SiO_4 were found to be largely pressure independent at room temperature. If, on the other hand, the pressure dependences of the bulk and shear modulus of the β phase of Mg_2SiO_4 are assumed to be identical to those for the α phase, the room temperature velocity contrasts between the two phases decrease by 20% and 12% from 1 bar to 13.8 GPa for compressional and shear waves, respectively.

Introduction

The elastic properties of minerals at elevated pressure are needed for a variety of geophysical purposes. Elastic moduli can be used to help place constraints on mantle composition through comparison with seismic data. In particular, elastic constant measurements are the only means to obtain information about the shear properties of minerals. The effects of pressure on the seismic wave anisotropy of mantle constituents have not been investigated in detail to date, although large changes in elastic anisotropy have been inferred from X ray diffraction measurements on a simple oxide (MgO) at relatively modest pressures [*Duffy et al.*, 1995a]. Such pressure-induced changes could have important implications for understanding the observed seismic anisotropy of Earth [e.g., *Meade and Silver*, 1995] Elastic properties also provide information on the structural properties of minerals and how their pressure-induced changes correlate with the overall mechanical properties of the solid. Furthermore, elastic moduli are sensitive indicators of certain phase transformations and provide information about interatomic forces. Finally, elasticity data provide an accurate means to constrain the compressibility.

Forsterite, α-Mg_2SiO_4, is the magnesian end-member of the olivine solid solution series and one of the most important silicates in Earth's upper mantle. Olivines of composition near $(Mg_{0.9},Fe_{0.1})_2SiO_4$ are found abundantly in peridotites derived from the upper mantle and are a major component in most mineralogical models of the upper mantle [e.g., *Ringwood*, 1975]. The compound Mg_2SiO_4 is stable in the olivine structure at ambient conditions. At higher pressures and temperatures it transforms to the wadsleyite structure, also known as β-Mg_2SiO_4. The temperatures and pressures of this transformation are not well determined because of experimental difficulties, but along Earth's geotherm it appears to occur around 13.8 GPa and 1300–1500 K [*Bina and Helffrich*, 1994]. The transformation is considered to be the origin of the 410-km seismic discontinuity. Owing to slow kinetics at room temperature the forsterite structure persists metastably to 50 GPa, above which (50 GPa $< P <$ 70 GPa) it partially transforms to an amorphous state [*Durbin et al.*, 1993; *Andrault et al.*, 1995]. The α-β transformation mechanism has been the subject of considerable controversy, in particular, whether it is martensitic or nucleation and growth type. It has been proposed that in the case of the martensitic transformation mechanism the transformation would be accompanied by a softening of the shear elastic moduli [*Poirier*, 1981]. The transformation mechanism is strongly dependent on the stress state of the sample [*Burnley and Green*, 1989].

Models for the structure and chemical composition of Earth's mantle have been inferred largely from the comparison between limited experimental results and seismic observations [*Anderson and Bass*, 1984; *Bass and Anderson*, 1984; *Bina*, 1993; *Bina and Wood*, 1987; *Duffy and Anderson*, 1989; *Gwanmesia et al.*, 1990; *Ita and Stixrude*, 1992; *Weidner*, 1985]. Although it is well understood that the most direct way to place constraints on the models is to compare the sound velocities and elasticity of candidate materials measured under high P-T conditions with the seismic observations, very few of the former have been available to date. The precision of the latter has increased with recent improvements in seismological methods [*Nolet et al.*, 1994].

Brillouin scattering is an optical technique in which acoustic velocities are determined from the frequency shift of laser light scattered by thermally generated acoustic waves. Application of Brillouin scattering at ambient pressure to minerals relevant to Earth's mantle was pioneered by *Weidner* [1975] and col-

[1]Now at Consortium for Advanced Radiation Sources, University of Chicago, Chicago, Illinois.

Copyright 1996 by the American Geophysical Union.

Paper number 96JB01266.
0148-0227/96/96JB-01266$09.00

Table 1. Experimental Conditions

P, GPa	Pressure Medium	Number of Velocities	RMS, km/s	Crystal	Density, g/cm^3
3.1	Ar	54	0.031	2	3.302
6.1	Ar	54	0.024	2	3.374
9.6	ME	79	0.055	1, 3	3.435
10.5	He	48	0.056	1	3.463
12.2	ME	48	0.049	1	3.503
15.1	He	51	0.052	1	3.558
16.2	He	36	0.042	1	3.582

ME, methanol-ethanol mixture. The density was not measured at 12.2 GPa but was calculated from the equation of state [*Downs et al.*, 1996]. Crystals 1 and 2 were polished near the "cubic (111)" plane. Crystal 3 was polished in the bc plane.

leagues and has provided much of our knowledge of the elastic properties of the phases that are assumed to dominate Earth's interior. Application of this technique to minerals at high pressure in a diamond cell was first carried out by *Shimizu et al.* [1982], who demonstrated that Brillouin spectra could be obtained from forsterite samples at pressures up to 4 GPa. This pioneering study was complicated by the low orthorhombic symmetry, and only six of the nine elastic moduli were determined. Few other subsequent elastic moduli measurements have been carried out at high pressure in diamond cells because of experimental difficulties and the time-consuming nature of the experiments. In recent years, however, there have been renewed efforts to obtain elastic moduli at high pressure, and several high-symmetry (isotropic, cubic, and hexagonal) systems have been studied [*Shimizu et al.*, 1995; *Zha et al.*, 1993, 1994]. Another recent development is the use of impulsive stimulated scattering (ISS) to obtain elastic moduli of low-symmetry materials at high pressure in diamond cells [*Zaug et al.*, 1993]. There have also been recent advances in the use of ultrasonic techniques in the large volume press [*Yoneda and Morioka*, 1992; *Li et al.*, 1996].

In this study, Brillouin scattering is used to obtain all nine elastic moduli of α-Mg_2SiO_4 forsterite at seven pressures between 3 and 16 GPa. We demonstrate that all the elastic moduli of this orthorhombic material can be obtained from measurements restricted to a single plane of the sample. This technique opens the way to study the pressure derivatives of sound velocity and elasticity for many possible Earth-forming materials. Because of the small sample size allowable in the light-scattering experiment, this technique is well-suited for measurements in this pressure range. The application of gas-pressure media ensures that the sample experiences a quasi-hydrostatic stress condition. Single-crystal X ray diffraction was also used to measure crystal orientation and density at each pressure and provides an independent measure of the isothermal equation of state. From the individual elastic moduli the aggregate bulk and shear modulus, equation of state, and thermodynamic properties to transition zone pressures have been obtained. The aggregate sound velocities, which can be compared with seismic observations, offer crucial information in constraining mantle composition.

Experimental Method

Forsterite, as an orthorhombic crystal, has nine symmetrically distinct elastic moduli [*Musgrave*, 1970]. Any phonon direction that is not perpendicular to a crystal axis of an orthorhombic structure will include information on all nine elastic moduli. For each phonon direction, three acoustic wave vectors can be obtained: one longitudinal (P wave) and two transverse (S wave). Mathematically, nine acoustic velocity measurements are sufficient to determine the nine elastic moduli, but to obtain better constraints on the individual moduli, many more measurements are typically used. It was found experimentally that the scattered light intensity for each of the three waves varies with respect to the angles between the phonon direction and each crystal axis. In fact, in the planes formed by the crystal axis the intensity of one of the shear modes can be diminished to undetectable levels. We found that the most favorable crystal plane for measurements is that in which an equel angle is made with each crystal axis. This plane can be described in reciprocal space by the real vector ($|a|$ $|b|$ $|c|$) and we refer to it as the "cubic (111)" plane.

Samples of synthetic end-member forsterite, synthesized near the turn of the century at the Geophysical Laboratory [*Allen et al.*, 1906], were donated by H. S. Yoder Jr. The

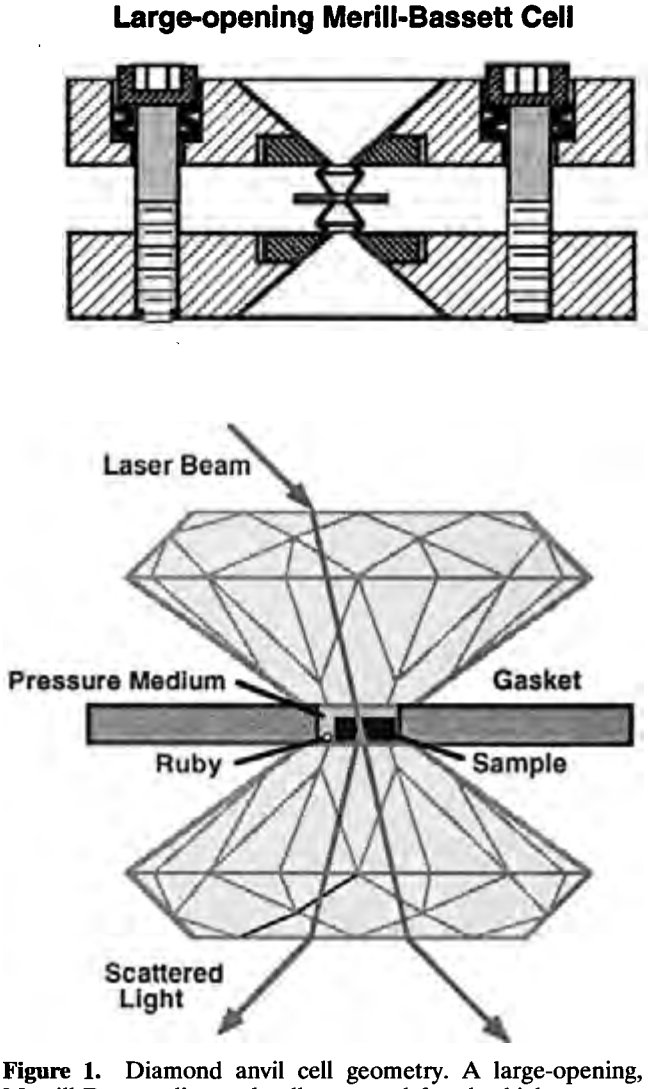

Figure 1. Diamond anvil cell geometry. A large-opening, Merrill-Bassett diamond cell was used for the high-pressure Brillouin scattering. A piece of well-polished single crystal, a pressure medium, and a few ruby chips were loaded in the gasket hole.

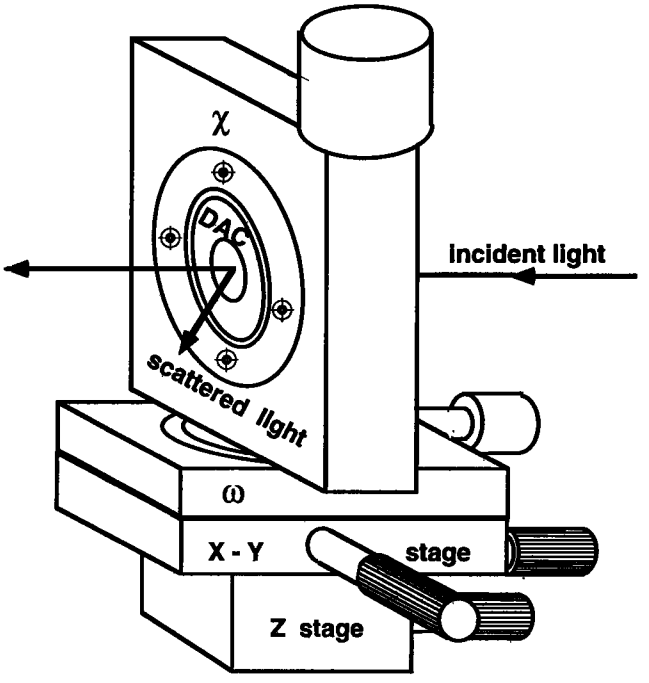

Figure 2. Diamond cell mount assembly. The sample platelet is coplanar with the diamond surface and the χ circle. A symmetric scattering geometry locates the phonon direction at the sectional line of the χ plane and scattering plane that eliminates the need to know the sample refractive index. By turning the χ circle, sound velocities corresponding to different phonon directions can be measured.

composition was determined with a JRA-8900L electron probe microanalyzer and confirmed to be pure Mg_2SiO_4. We polished two pieces of the sample to platelet shapes with the surfaces parallel to the plane discussed above. One piece was polished to a thickness of 18 μm and was used for measurements at pressures of 9.6, 10.5, 12.2, 15.1, and 16.2 GPa. Another piece was polished to a thickness of 55 μm and was used at 3.1 and 6.1 GPa. Three pressure media, Ar, He, and a 4:1 mixture of methanol-ethanol, were used in different pressure ranges to avoid overlap of Brillouin peaks and to ensure quasi-hydrostatic pressure conditions (Table 1). A modification of the large-opening, Merrill-Bassett diamond anvil cell [*Mao and Bell*, 1980] was used for the high-pressure Brillouin scattering measurements (Figure 1). The sample platelet was loaded into the gasket hole with one of its parallel surfaces placed against the diamond culet. In each run a few chips of ruby were mounted next to the sample. The sample position was fixed by the frozen gas or highly viscous fluid medium, and no changes due to gravitational forces were detected during the measurement period, which may be several weeks duration at a given pressure.

Figure 2 shows the diamond cell stage assemblage. The degrees of freedom of the diamond anvil cell are x, y, z translations and ω, χ rotations. The translations are used to move the sample to the correct position for the scattering measurement; ω rotation was used for setting the scattering geometry; and χ rotation was used for selecting the phonon direction in the platelet crystal plane. The newly designed high-pressure Brillouin scattering system [*Zha et al.*, 1993] is shown in Figure 3. The main component is the Sandercock-

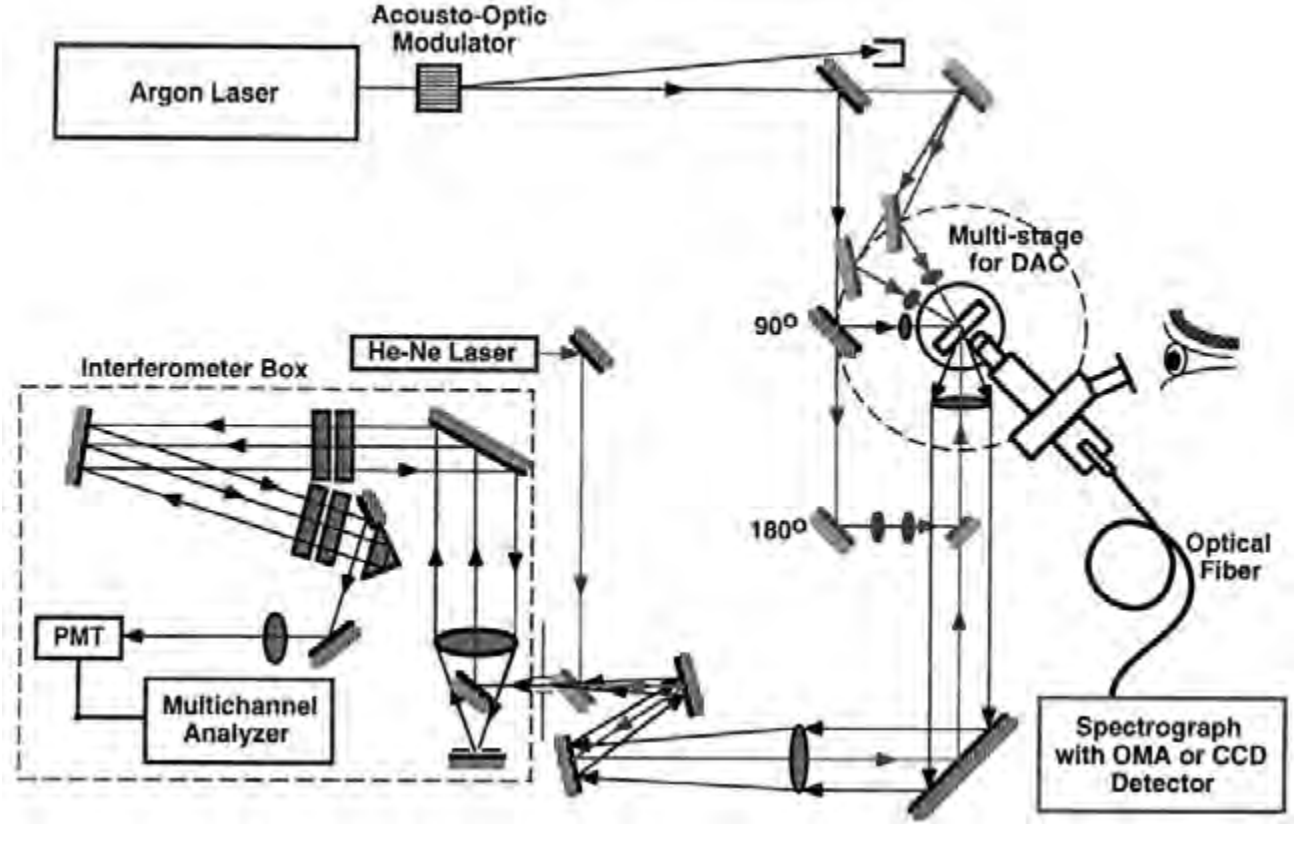

Figure 3. Diagram of experimental setup.

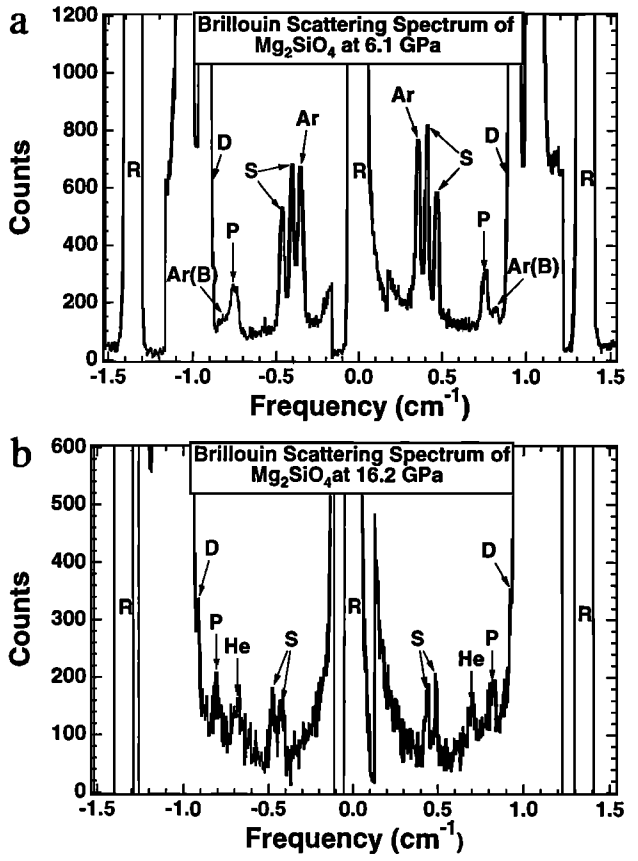

Figure 4. (a) Brillouin spectrum at 6.1 GPa with Ar medium. (b) Brillouin spectrum at 16.2 GPa with He media. R, Rayleigh peak; D, diamond peak; Ar, argon peak; Ar(B), argon *P* wave backscattered from diamond surface; He, helium peak; S, sample shear waves; *P* sample *P* wave.

type six-path interferometer [*Mock et al.*, 1987]. A single-frequency argon-ion laser was used as an excitation source. An acousto-optic modulator is used to depress the Rayleigh peak intensity, which occurs when its ultrasonic deflection field is synchronized with interferometer scanning settings. The system was designed to allow for facile changes between different scattering geometries. A portable microscope-optical fiber-spectrograph system is used for in situ pressure and temperature (blackbody radiation, not used in this experiment) measurements. A He-Ne laser is used for alignment and setting the scattering angle.

The crystallographic orientation and density were determined at each pressure by X ray diffraction with a Picker four-circle X ray diffractometer. The crystallographic orientation is then used in the Brillouin scattering measurement for the calculation of the direction cosine for each phonon direction. Attention was paid to the pressure environment of the sample. Broadening of the X ray peaks indicated that the sample may have experienced nonhydrostatic stress from bridging by the diamond anvils, by contact with edges of the gasket hole, or by a nonhydrostatic pressure medium [*Downs et al.*, 1996].

All of the data in this experiment were collected with a symmetric 100° scattering geometry, where the angle refers to that between incident beam and scattered light outside of the diamond cell. With this geometry, the Brillouin frequency shift $\Delta\nu$ of an optically isotropic material is related to the acoustic velocity V and incident laser wavelength λ_0 by

$$V = \Delta\nu\lambda_0/2\sin 40° \quad (1)$$

where 40° is the angle between the laser beam and the diamond cell axis outside of the diamond cell. The uncertainties in phonon directions and sound velocities introduced by using this expression for a material with weak optical anisotropy are small and well within the experimental errors.

We also used a third sample platelet polished in the b-c plane, which was loaded in a separate diamond cell but measured at the same pressure as one of the other points (9.6 GPa). This sample gave only four elastic moduli (C_{22}, C_{33}, C_{44}, C_{23}) as we could obtain only one shear mode in this plane. The sample polished along the cubic (111) plane gives a complete set of elastic moduli, as every measurement for each phonon direction gives three wave modes. Even though the birefringence corresponding to the two samples is different, the elastic moduli data from the two samples are consistent whether the sound velocity data measured from those two samples were fitted separately or together.

Results

Sound Velocities

Figure 4 shows the Brillouin spectra collected at 6.1 GPa and 16.2 GPa, respectively. The sample thickness and refractive index contrast between the pressure medium and the sample have a large effect on the quality of the spectra. Increasing the scattering volume enhances the signal-to-noise ratio. A large refractive index contrast between the sample and pressure medium also reduces the signal-to-noise ratio. For phonons propagating in the cubic (111) plane, we always obtain three sound waves for every phonon direction, although the individual peak intensity may change with orientation. In contrast to solid hydrogen [*Zha et al.*, 1993], the intensities of the *P* wave peaks are generally weaker than those of the *S* waves, and they have similar intensities only for very small angular ranges. Ten to 18 phonon directions were measured at each pressure, and these supplied sufficient sound velocity data for calculating all nine elastic moduli solely from measurements in a single-crystal plane.

Figure 5 shows the sound velocity distribution in the platelet crystal plane at 6.1 GPa and 16.2 GPa. The solid lines are calculated sound velocities from the best fit elastic moduli. The root-mean-square (RMS) deviation between measured and calculated velocities is 0.02 km/s at 6.1 GPa and 0.04 km/s at 16.2 GPa (Table 1). With increasing pressure, both longitudinal and transverse sound velocities increase. The anisotropy of the longitudinal mode shows no significant change, in contrast to the behavior of the transverse modes (Figure 5). This difference in behavior may be related to the different compressibilities of different crystal axes. It is also reflected in the different pressure derivatives of individual elastic modulus (Figure 6).

Elastic Moduli

Christoffel's equation relates acoustic velocities to crystallographic direction and the elastic moduli [*Musgrave*, 1970; *Every*, 1980]:

$$\det|\Gamma_{ik} - \rho V^2\delta_{ik}| = 0 \quad (2)$$

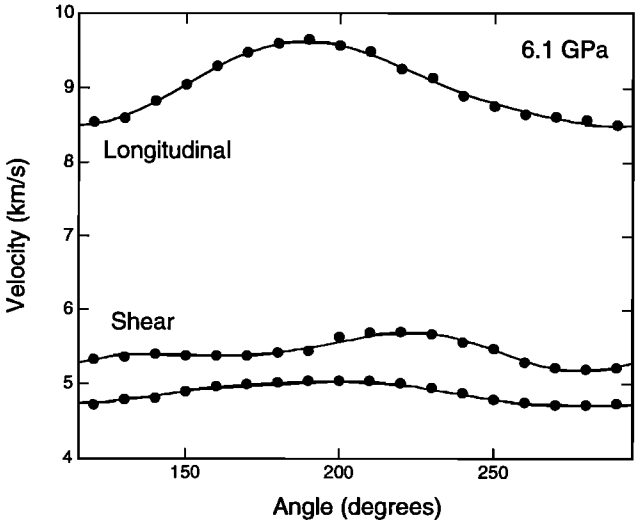

Figure 5a. Compressional and shear acoustic velocities as a function of χ angle (about an arbitrary setting mark on the diamond cell) at 6.1 GPa. Solid lines are calculated from best fit elastic moduli. The RMS deviation between calculated and measured velocities is 24 m/s.

where ρ is the density, V is the sound velocity, and δ_{ik} is a delta function (i.e., when $i = k$, $\delta_{ik} = 1$; when $i \neq k$, $\delta_{ik} = 0$). The Kelvin-Christoffel stiffness Γ_{ik} is

$$\Gamma_{11} = n_1^2 C_{11} + n_2^2 C_{66} + n_3^2 C_{55} \quad (3)$$

$$\Gamma_{22} = n_1^2 C_{66} + n_2^2 C_{22} + n_3^2 C_{44} \quad (4)$$

$$\Gamma_{33} = n_1^2 C_{55} + n_2^2 C_{44} + n_3^2 C_{33} \quad (5)$$

$$\Gamma_{23} = n_2 n_3 (C_{23} + C_{44}) \quad (6)$$

$$\Gamma_{13} = n_1 n_3 (C_{13} + C_{55}) \quad (7)$$

$$\Gamma_{12} = n_1 n_2 (C_{12} + C_{66}) \quad (8)$$

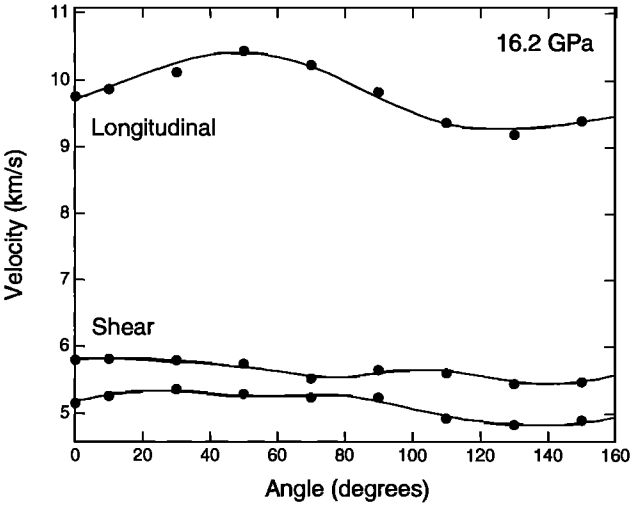

Figure 5b. Same as Figure 5a except at 16.2 GPa. The RMS deviation between calculated and measured velocities is 42 m/s.

the n_i and C_{ij} are direction cosines of measured phonons and elastic moduli, respectively. The direction cosines are determined by the three Eulerian angles that relate the laboratory and crystal reference frames by

$$n_1 = \cos\theta \cos\chi \cos\varphi - \sin\chi \sin\varphi$$

$$n_2 = -\cos\theta \cos\chi \sin\varphi - \sin\chi \cos\varphi$$

$$n_3 = \sin\theta \cos\chi.$$

The matrix equation (2) has three roots for sound velocities which correspond to a longitudinal and two transverse modes. Using the density from the X ray measurement and the measured sound velocities from Brillouin scattering, we can obtain the C_{ij} and the Eulerian angles by using a nonlinear least

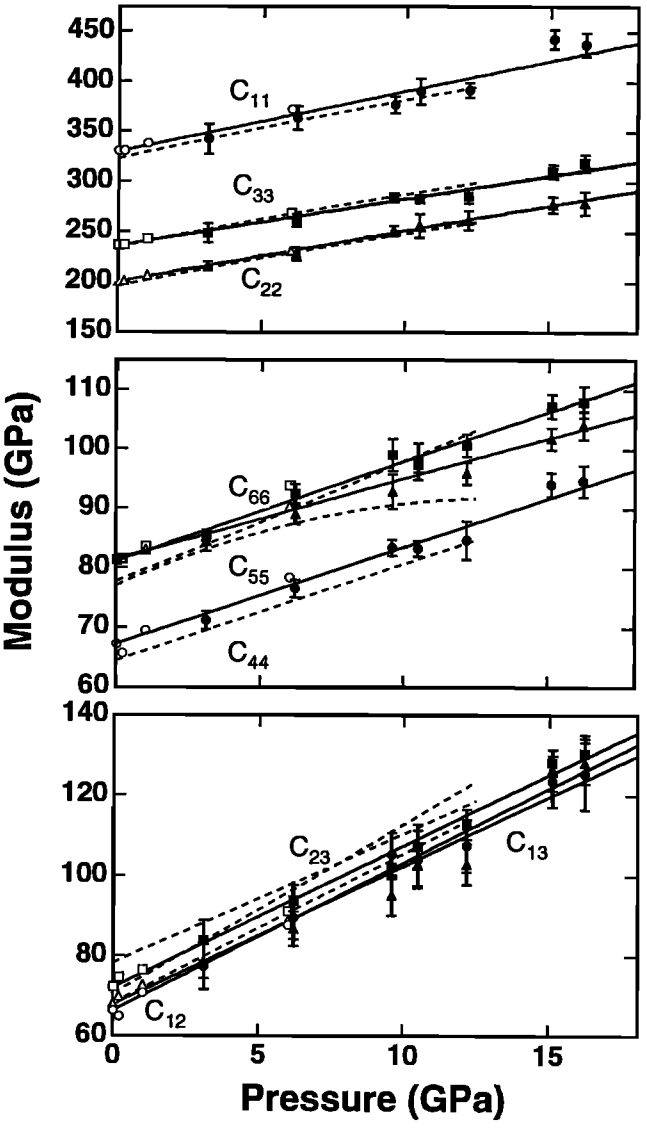

Figure 6. Elastic moduli of forsterite as a function of pressure. Solid symbols with error bars (2σ) are data of this study. Solid lines are least squares fits to present data combined with ambient P data [*Isaak et al.*, 1989]. The open symbols show the results of ultrasonic studies of forsterite [*Kumazawa and Anderson*, 1969; *Graham and Barsch*, 1969; *Yoneda and Morioka*, 1992] at the highest reported pressure. The dashed lines are fits to the ISS results [*Zaug et al.*, 1993].

Table 2. Elastic Moduli of Forsterite

P	C_{11}	C_{22}	C_{33}	C_{44}	C_{55}	C_{66}	C_{12}	C_{13}	C_{23}
3.1	341.93±7.51	215.69±2.36	248.46±4.85	71.14±0.75	84.35±0.82	85.10±0.65	77.23±2.80	78.50±2.10	83.73±2.53
6.1	363.27±5.98	227.84±3.19	261.37±3.26	76.52±0.73	89.01±0.83	92.43±0.82	89.42±2.68	86.62±2.16	93.69±2.05
9.6	376.59±4.21	251.16±2.21	284.48±2.31	83.40±0.69	92.83±1.44	98.98±1.37	105.34±2.68	95.12±2.55	104.09±1.42
10.5	390.54±6.50	256.18±5.93	283.18±2.02	83.28±0.66	97.34±0.65	97.94±1.54	104.17±3.60	102.96±2.66	107.28±2.79
12.2	391.56±3.71	261.67±4.84	286.02±3.70	84.67±1.60	95.93±0.95	100.69±0.97	107.53±3.26	102.96±2.55	112.77±1.88
15.1	443.15±4.82	277.74±4.05	310.93±3.36	94.03±0.99	101.80±0.95	107.34±1.01	123.55±3.19	126.42±2.56	128.28±1.62
16.2	437.18±5.94	279.11±5.82	319.47±4.02	94.66±1.32	104.04±1.19	108.05±1.31	125.40±4.45	128.19±2.56	130.52±2.32

In units of gigapascals.

squares inversion [*Press et al.*, 1987] of closed-form solutions to the Christoffel equation [*Every*, 1980]. An uncertainty of ±0.5% is assigned to the individual acoustic velocity measurements. The elastic moduli C_{ij} as a function of pressure are shown in Figure 6 and Table 2. All C_{ij} increase linearly with pressure but with different slopes. The elastic moduli are constrained to ±1–3% (1σ), and the angles are constrained to ±2°.

Elastic moduli reported in previous studies are also shown in Figure 6. The open symbols show the results of a previous ambient pressure study [*Isaak et al.*, 1989] and high-pressure ultrasonic studies [*Graham and Barsch*, 1969; *Kumazawa and Anderson*, 1969; *Yoneda and Morioka*, 1992] at the highest pressure achieved in each of these studies. Our results are generally in good agreement with the results of *Yoneda and Morioka* [1992] near 6 GPa. The dashed lines show fits to the elastic moduli reported using the ISS technique [*Zaug et al.*, 1993] for a sample of San Carlos olivine (10 mol % Fe). Taking into account differences in composition, the ISS results are generally consistent with the present study, with the exception of C_{55}. Our results indicate that C_{55} remains a linear function of pressure up to 16 GPa, whereas a strong nonlinearity is observed for this modulus in the ISS data. The reason for this discrepancy is unclear at present and is a subject of continuing investigation.

In this study we have shown that it is possible to recover the orientation as well as elastic moduli for sound velocity data on an orthorhombic crystal restricted to a single-crystal plane. Previously, this has been accomplished only for high symmetry systems (cubic) [e.g., *Shimizu and Sasaki*, 1992]. The orientations were determined using the X ray values as starting models, and differences of a few degrees between starting and final angles were usually found. The differences may reflect experimental error as well as uncertainty in parallelism and flatness. As discussed in the appendix, such errors do not contribute significantly to errors in the measured acoustic velocities.

We have used Monte Carlo simulations to examine the reliability of elastic moduli determinations from single-plane sound velocity data. Artificial data sets were constructed by computing sound velocities at 10° intervals in the cubic (111) plane from a known set of elastic moduli. The velocities were then perturbed by amounts up to ±1% using a random number generator. One thousand artificial data sets were computed in this manner. Each data set was then inverted (the direction cosines were fixed in these calculations) and the elastic moduli were obtained. For the longitudinal and shear moduli (C_{11} thorugh C_{66}), the recovered elastic moduli were within ±5% of the known starting values in nearly all (>95%) cases. The errors in the recovered off-diagonal moduli (C_{12}, C_{13}, and C_{23}) could be larger but were within ±10% of the starting values in all cases. The scatter in the recovered elastic moduli values is due to both random errors in the velocities and to trade-offs among pairs of elastic moduli. The latter is a consequence of the lack of any pure mode propagating directions in the single-plane data. It is expected that trade-off errors would tend to cancel when the elastic properties are averaged to obtain the properties of a random polycrystalline aggregate. This conclusion is borne out by the Monte Carlo simulations. The Voigt-Reuss-Hill bulk moduli obtained from the 1000 simulations are in nearly all cases within ±3% of the expected value, despite the larger errors in the individual moduli. The aggregate shear modulus is better resolved; it falls within ±2% of the expected values in all cases. The aggregate P and S wave velocities are within 1% of the expected values in all cases. Thus, despite the limitations in our ability to recover the individual moduli by this method; we expect that the aggregate moduli and sound speeds are well-determined.

The choice of the cubic (111) plane is advantageous for another reason as well. By analyzing data for 14 orthorhombic silicates in which the full set of elastic moduli have been measured, we find that the VRH compressional and shear wave velocities in such materials are typically quite close to the arithematic average of their respective velocities in the cubic (111) plane. The average compressional velocity in this plane is always within 3% of the VRH average and in most cases is about 1% larger than the aggregate P wave velocity for the measured silicates. Similar results hold for the shear waves.

Table 3. Aggregate Elastic Properties of Forsterite

P, GPa	K_S, GPa	G, GPa	σ	V_P, km/s	V_b, km/s	V_S, km/s
3.1	140.75±2.03	84.48±1.42	0.250±0.005	8.76±0.05	6.53±0.05	5.06±0.04
6.1	152.42±2.24	88.97±1.47	0.256±0.005	8.96±0.05	6.72±0.05	5.14±0.04
9.6	167.19±1.85	94.34±1.22	0.263±0.003	9.24±0.05	6.98±0.04	5.24±0.04
10.5	170.98±2.21	95.42±1.32	0.265±0.004	9.28±0.05	7.03±0.05	5.25±0.04
12.2	174.29±1.91	95.98±1.34	0.267±0.003	9.92±0.05	7.05±0.04	5.23±0.04
15.1	195.51±3.19	102.58±1.63	0.277±0.004	9.66±0.06	7.41±0.06	5.37±0.04
16.2	197.54±2.91	103.31±1.48	0.277±0.004	9.67±0.06	7.43±0.06	5.37±0.04

Thus, even without information on the crystal orientation within this plane, averaged velocities are typically close to the aggregate velocity of silicates. These averages are likely to be a reflection of the fact that this plane effectively samples all of the elastic moduli in roughly equal proportions.

Aggregate Properties

There is no general solution to the problem of calculating the properties of a randomly oriented polycrystalline aggregate from the single-crystal properties; however, there are well-established bounding procedures. Aggregate properties were obtained from the individual moduli by taking orientational averages using the Voigt-Reuss-Hill procedure [*Watt and Peselnick*, 1980] (Table 3). Figure 7 shows the pressure dependencies for the bulk modulus and shear modulus. Also shown in Figure 7 are ultrasonic data for forsterite [*Graham and Barsch*, 1969; *Kumazawa and Anderson*, 1969; *Yoneda and Morioka*, 1992] and San Carlos olivine [*Webb*, 1989] as well as the more recent ISS data for San Carlos olivine [*Zaug et al.*, 1993]. We find that K_S is independent of Fe content at high pressure. However, the shear modulus is offset and displays a different pressure dependence in the ISS data and this study. For San Carlos olivine a nonlinearity is clearly observed in the shear modulus at high pressure, whereas the modulus is linear with pressure within the resolution of our data on forsterite. This nonlinearity is attributable to the differing behavior of the C_{55} modulus.

The potential effect of different pressure media on the compression properties of forsterite has been addressed elsewhere [*Downs et al.*, 1996]. It is worthwhile to examine how these might effect the elastic properties as well. The datum at 12.2 GPa was recorded in methanol-ethanol medium that is frozen at this pressure and may have appreciable shear strength. X ray diffraction peaks at this pressure were broadened to the extent that the compression data are not considered reliable [*Downs et al.*, 1996]. This could explain why the aggregate bulk and shear modulus at this pressure lie somewhat below the trend of the rest of the data. There was no compelling reason, however, to discard the data on the basis of the Brillouin measurements, so we elected to include it in the analysis. A second issue is that there is evidence from X ray data on partially decompressed samples that He could be diffusing through the defect structure of the crystal [*Downs et al.*, 1996]. It is not clear at present whether this could affect the high-pressure elastic properties, but there is at present no evidence from Brillouin or X ray data of anomalous behavior of such materials held in a helium pressure medium during compression. The scatter of the data in Figure 7 may therefore reflect effects of the use of differing pressure media to some degree.

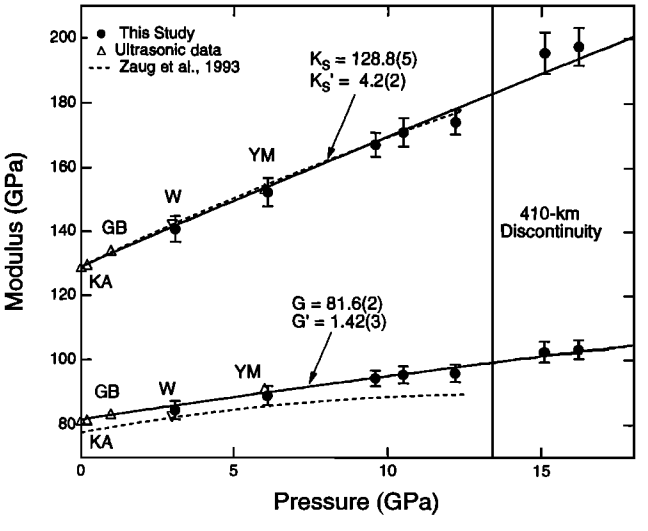

Figure 7. Aggregate bulk and shear modulus of forsterite as a function of pressure. Inverted triangle shows the results of ultrasonic data to 3 GPa for San Carlos olivine [*Webb*, 1989]. Other symbols are the same as in Figure 6. Solid lines are from finite strain fits to present and ambient pressure data [*Isaak et al.*, 1989]. The vertical line shows the approximate pressure of the 410-km seismic discontinuity. Primes indicate first pressure derivatives of the aggregate moduli. The abbreviations are as follows: KA, *Kumazawa and Anderson* [1969]; GB, *Graham and Barsch* [1969]; W, *Webb* [1989]; YM, *Yoneda and Morioka* [1992].

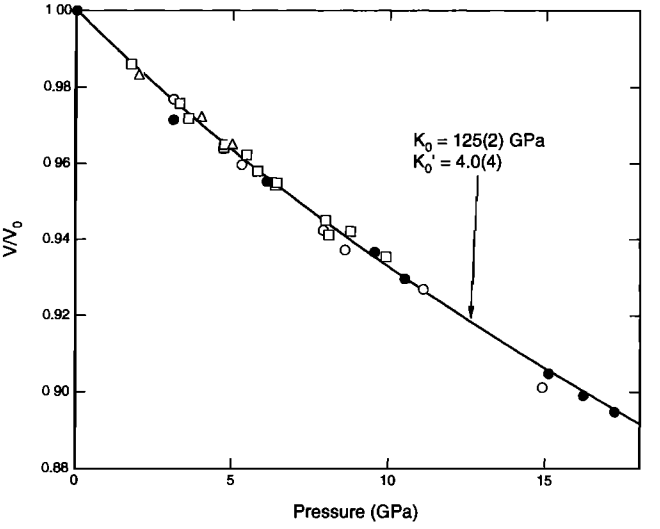

Figure 8. Static compression data for forsterite from this and other studies. The solid symbols and line are the present data and a third-order Birch-Murnaghan equation fit, respectively. Other data are from *Olinger* [1977] (squares), *Kudoh and Takeuchi* [1985] (circles), and *Hazen* [1976] (triangles).

Volume-pressure data for forsterite from this and previous studies are shown in Figure 8. A third-order Birch-Murnaghan fit to the present static compression data yields an isothermal bulk modulus of 125 ± 2 GPa and a pressure derivative of 4.0 ± 0.4. This is in good agreement with the parameters for the adiabatic bulk modulus determined here from Brillouin data. An equation of state determined from the Brillouin data predicts volumes in agreement with those measured by X ray diffraction, thereby demonstrating the self-consistency of our results. It is also of interest to note that our measured volumes near 15 GPa (using a He medium) are significantly greater than the previous result near this pressure taken in an alcohol medium. The more nearly hydrostatic pressure environment of our sample should provide a better determination of the volume at this pressure. Further analysis of the X ray diffraction results is given by *Downs et al.* [1996].

A comparison of the aggregate bulk and shear modulus of forsterite measured in this study with third- and fourth-order finite strain extrapolation [*Davies and Dziewonski*, 1981] of lower pressure data is shown in Figure 9. The work of

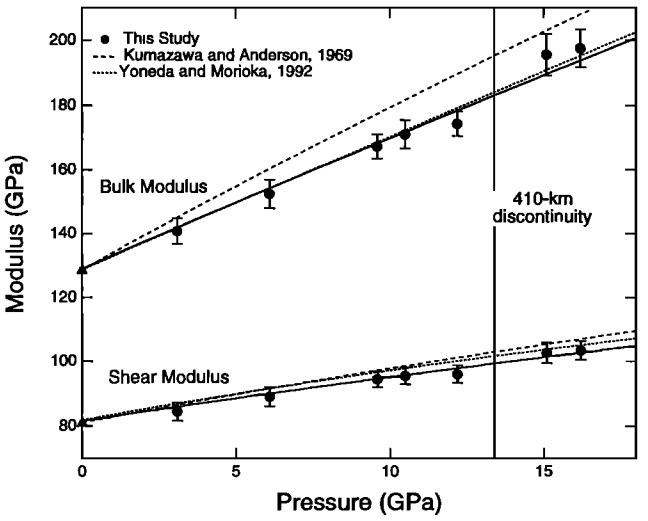

Figure 9. Comparisons of present determinations of adiabatic bulk and shear modulus of forsterite with extrapolations using finite strain theory of lower-pressure data.

Kumazawa and Anderson [1969] was performed to a maximum pressure of 0.2 GPa, whereas *Yoneda and Morioka* [1992] (Table 4) reached a peak pressure of 6 GPa. The pressure derivatives of the individual elastic moduli determined by *Kumazawa and Anderson* [1969] are all 20–40% higher than our values. Thus systematic errors in pressure calibration may be responsible for the higher elastic moduli determined in previous very low pressure studies. Our results are in better agreement with extrapolations (fourth-order finite strain) of the ultrasonic data of *Yoneda and Morioka* [1992].

Discussion

The 410-km seismic discontinuity in the mantle is believed to be due to the α-β phase change in $(Mg,Fe)_2SiO_4$ [*Ringwood*, 1975]. The amount of olivine in the transition zone could be determined by comparing laboratory measurements of the acoustic velocity contrast between the two phases with seismic velocity data. At ambient pressure, the velocity contrasts for P and S waves are 12.9% and 14.0%, respectively. Seismic velocity contrasts across the discontinuity are about 4–5% [*Nolet et al.*, 1994]. Thus the laboratory data are consistent with a mantle olivine fraction of about 29–39% if the velocity contrast is independent of P and T. Sound velocities of the wadsleyite phase of Mg_2SiO_4 were measured on a polycrystalline aggregate to 3 GPa [*Gwanmesia et al.*, 1990]. Using these data together with early ultrasonic data [*Graham and Barsch*, 1969] for the pressure dependence of the velocities in forsterite, it was concluded that the velocity contrast across the transition is a strongly decreasing function of pressure at room temperature [*Gwanmesia et al.*, 1990]. Using our new values for the elasticity of forsterite, however, we find that the velocity contrast is largely independent of pressure (Figure 10). At 13.8 GPa the room temperature velocity contrasts across the α-β transition for P and S waves are 12.0% and 13.9%, respectively. A seismic discontinuity of 4–5% in magnitude would therefore require a forsterite fraction of 0.37 ± 0.04 (P waves) or 0.32 ± 0.03 (S waves). This calculation ignores many important factors (temperature, Fe content, texture, element partitioning) and assumes the discontinuity is entirely due to the α-β phase change. The high-pressure acoustic velocities in the phases of Mg_2SiO_4 are consistent with olivine contents that are significantly below that found in the pyrolite model (60% olivine) for the upper mantle [*Ringwood*, 1975]. If the pressure derivatives of β phase reported by *Gwanmesia et al.* [1990] are overestimated, the allowed olivine content of the mantle increases. Assuming the pressure derivatives of the two phases are identical ($K' = 4.2$, $G' = 1.4$), the velocity contrasts at 13.8 GPa become 10.3% (P waves) and 12.3% (S waves) (Figure 10). This is consistent with an olivine fraction of 0.44 ± 0.05 (P waves) and 0.37 ± 0.04 (S waves). Thus current room temperature elasticity data for the Mg_2SiO_4 system suggest that mantle olivine fraction required to satisfy seismic data at 410-km depth is about 0.3–0.5. Further discussion of the implications of these results for mantle composition is reported elsewhere [*Duffy et al.*, 1995b].

Table 4. Pressure Derivatives From High-Pressure Studies of Mg-Rich Olivines

Study	X-Mg	P_{max}, GPa	K'	K'', GPa^{-1}	G'	G'', GPa^{-1}
Kumazawa and Anderson [1969]	1.0	0.2	5.4	···	1.8	···
Graham and Barsch [1969]	1.0	1.0	5.0	···	1.8	···
Webb [1989]	0.91	3.0	4.66	−0.15	1.96	−0.11
Yoneda and Morioka [1992]	1.0	6.0	4.2	−0.018	1.7	−0.44
Zaug et al. [1993]	0.90	12.5	4.56	−0.10	1.71	−0.12
This study	1.0	16.2	4.2	···	1.4	···

Single and double primes are first and second pressure derivatives of the moduli, respectively.

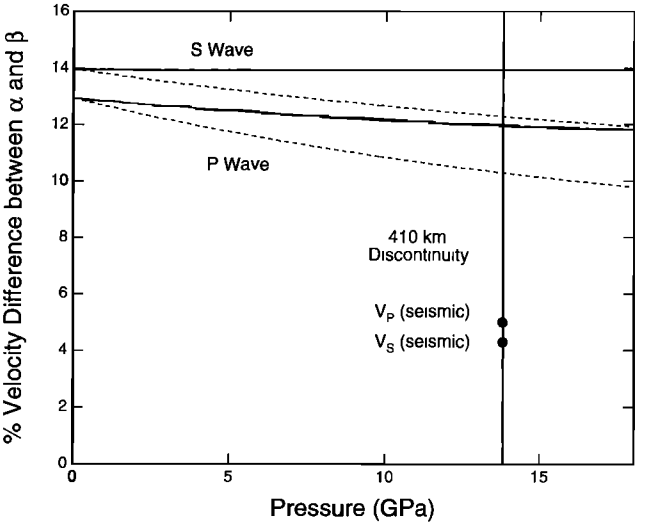

Figure 10. The velocity contrast between the α and β phases of Mg_2SiO_4 as a function of pressure at room temperature. Solid lines are results of this study together with the β phase data of *Gwanmesia et al.* [1990]; dashed lines are calculated assuming the pressure derivatives of the β phase are the same as for the α phase. The vertical line shows the pressure of the 410-km seismic discontinuity (13.8 GPa).

Summary

We report measurement of the pressure dependence of the complete set of elastic moduli for forsterite up to transition zone pressures by use of Brillouin scattering spectroscopy, diamond anvil cell techniques. We have shown for the first time that the cubic (111) plane of an orthorhombic crystal (forsterite) can be used to obtain all the elastic moduli by measuring the sound velocity distribution only in this single plane. The pressure dependences of elastic moduli for forsterite vary linearly over this pressure range and are much lower than those extrapolated from previous measurements using ultrasonic techniques at much lower pressures. By combining our results with recent data for polycrystalline β-Mg_2SiO_4 (wadsleyite) up to 3 GPa we found the contrast in acoustic velocities between the two phases are not sensitive to pressure. That is, even at high pressure, the acoustic velocities in the phases of Mg_2SiO_4 are consistent with olivine contents that are significantly below that found in the pyrolite model (60% olivine) for the upper mantle [*Ringwood*, 1975]. Elastic moduli measurements of β-Mg_2SiO_4 over a similar pressure range are necessary, however, to constrain more reliably the olivine content of Earth's upper mantle.

Appendix: Errors Introduced by Nonparallel Diamond and Sample Surfaces

In this appendix we present an analysis of the error in the acoustic velocity determination due to errors in sample flatness and parallelism. First, we consider the case where the two sample surfaces are not parallel (Figure A1). The misalignment between the two sample surfaces is assumed to be small and is given by the angle $\Delta\alpha$. Assuming the upper surface of the sample is not parallel to the diamond anvils but the bottom surface is parallel, the laser beam traveling through the sample will be refracted by an angle χ from the diamond anvil cell axis. The scattered beam containing the Brillouin frequency shift will make an angle $\phi_2 + \Delta\alpha$ with the diamond cell axis. By applying Snell's law to the diamond-liquid interface and to interfaces between the liquid and the parallel and unparallel surfaces at the top of the sample, we obtain the following relations:

$$n_L \sin(\phi_1 + \Delta\alpha) = \sin 40° \quad \text{(A1)}$$

$$n_L \sin\phi_1 = n_S \sin(\chi - \Delta\alpha) \quad \text{(A2)}$$

$$n_L \sin(\phi_1 + \Delta\alpha) = n_S \sin(\phi_2 + \Delta\alpha) \quad \text{(A3)}$$

where n_L and n_S are the inices of refraction of the liquid and sample, respectively. These yield the following expressions for the angles:

$$\phi_1 = \sin^{-1}(0.6428/n_L) - \Delta\alpha \quad \text{(A4)}$$

$$\phi_2 = \sin^{-1}(0.6428/n_S) - \Delta\alpha \quad \text{(A5)}$$

$$\chi = \sin^{-1}(n_L \sin\phi_1/n_S) + \Delta\alpha \quad \text{(A6)}$$

The range of possible values for these angles can be determined using typical values for the parameters. The error in parallelism, $\Delta\alpha$, is can readily by controlled to less than 0.1° through the use of a piston-cylinder jig for polishing the sample. The refractive index of the liquid, n_L, will vary between 1.1 and 1.6 for typical media at these pressures. The sample refractive index n_S is between 1.7 and 1.9. Therefore ϕ_1 ranges

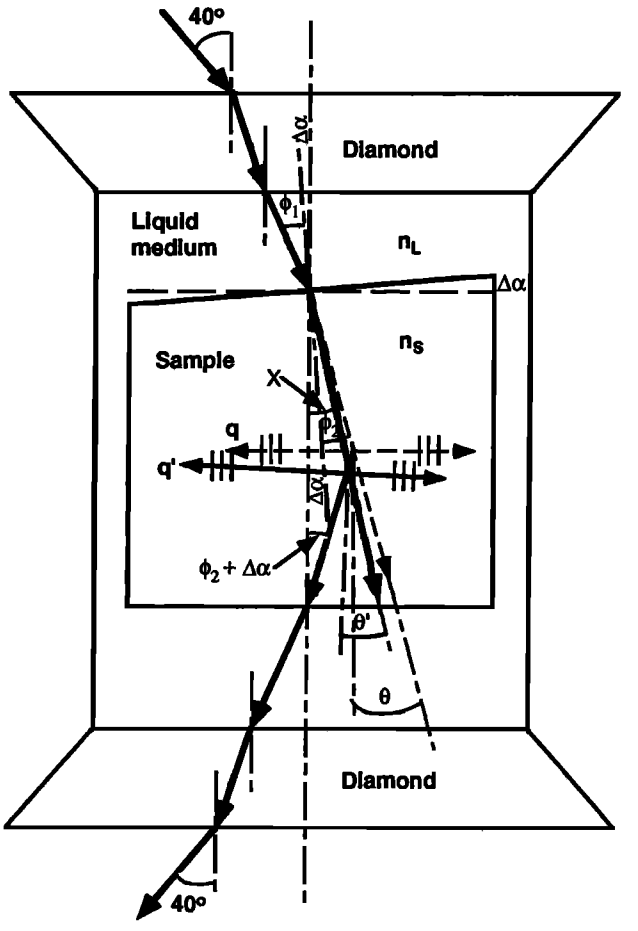

Figure A1. Light path through the diamond cell assembly when the sample surfaces are not parallel.

from 35.65° (n_L = 1.1) to 23.59° (n_L = 1.6). Similarly, ϕ_2 ranges from 22.12° (n_S = 1.7) to 19.67° (n_S = 1.9). The angle χ can then range from 22.26° to 19.79°. The half scattering angle θ for a sample with two parallel surfaces, $\theta = \phi_2 + \Delta\alpha$, ranges from 22.22° to 19.77°. When the samples surfaces are not parallel, the half scattering angle, $\theta' = (\chi + \phi_2 + \Delta\alpha)/2$, ranges from 22.24° to 19.78°. Thus the difference in phonon direction due to surfaces misaligned by less than one-tenth of a degree is less than or equal 0.02°. The velocity error resulting from this amount of mismeasurement of the phonon direction can be ignored. The error in calculated sound velocity is obtained by applying the formula $V = \Delta\nu\lambda/(2n_S \sin\theta)$ inside the sample (as oppossed to equation (1), where the expression is applied outside the diamond cell). The fractional error is found to be proportional to $(\sin\theta' - \sin\theta)/\sin\theta$ which is less than or equal to 0.1% for a parallelism deviation of less than 0.1°.

In the second case, we consider the situation where the sample surfaces are parallel to each other but they are not parallel to the diamond surfaces (Figure A2). To check the parallelism of sample and diamond surfaces, a white light beam incident upon the sample is used to produce a wedge interference pattern between the sample and diamond surface both before and after the pressure medium is loaded. In this way, the tilt angle $\Delta\alpha$ is easily controlled to less than 0.3°. As shown in Figure A2, the incidence angle of the scattered light at the interface between the bottom of the sample and the

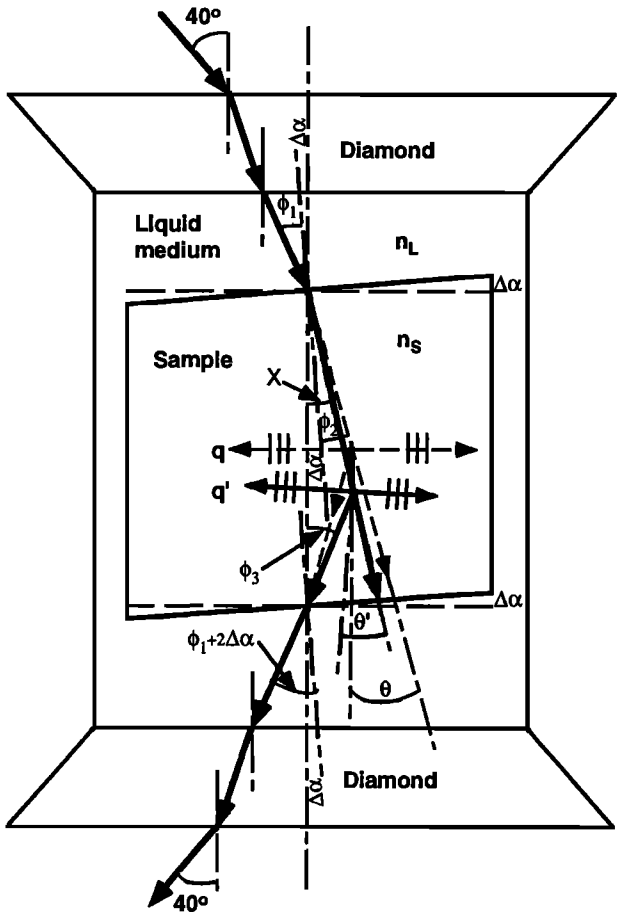

Figure A2. Light path through the diamond cell assembly when the sample surfaces are not parallel to the diamond surface.

liquid medium is $\phi_3 + \Delta\alpha$, and the refracted angle is $\phi_1 + 2\Delta\alpha$. The following expressions may be written by applying Snell's law:

$$n_L \sin(\phi_1 + \Delta\alpha) = \sin 40° = 0.6428$$
$$n_L \sin(\phi_1 + 2\Delta\alpha) = n_S \sin(\phi_3 + \Delta\alpha) \quad \text{(A7)}$$

Solving these expressions yields values for ϕ_1 between 35.46° (n_L = 1.1) and 23.39° (n_L = 1.6), while ϕ_3 ranges from 22.09° (n_S = 1.7) to 19.72° (n_S = 1.9). The angle χ can then range from 22.35° to 19.83°. The half scattering angle for parallel surfaces, $\theta = \phi_2 + \Delta\alpha$, ranges from 22.42° to 19.97°. When the sample and diamond surfaces are not parallel, the half scattering angle, $\theta' = (\chi + \phi_3)/2$, is between 22.22° and 19.78°. Thus the difference in phonon direction due to misalignment of the diamond and sample surfaces is ≤0.2°. The error in calculated sound velocity introduced by this angle differnce can be computed from the velocity equation above. The velocity error is ≤0.9% for angles errors ≤0.3°.

Acknowledgments. We thank Hatten S. Yoder Jr. for supplying the forsterite sample and reviewing the paper and Chris Hadidiacos for assistance with the sample microprobe analysis. Thanks are also given to Charles T. Prewitt, Robert M. Hazen, and Jay D. Bass for providing helpful comments. This work was supported by the NSF.

References

Allen, E. T., F. E. Wright, and J. K. Clement, Minerals of the composition $MgSiO_3$: A case of tetramorphism, *Am. J. Sci.*, *22*, 385–438, 1906.

Anderson, D. L., and J. D. Bass, Mineralogy and composition of the upper mantle, *Geophys. Res. Lett.*, *11*, 637–640, 1984.

Andrault, D., M. A. Bouhifd, J. P. Itie, and P. Richet, Compression and amorphization of $(Mg,Fe)_2SiO_4$ olivines: An x-ray diffraction study up to 70 GPa, *Phys. Chem. Miner.*, *22*, 99–107, 1995.

Bass, J. D., and D. L. Anderson, Composition of the upper mantle: Geophysical tests of two petrological models, *Geophys. Res. Lett.*, *11*, 237–240, 1984.

Bina, C. R., Mutually consistent estimates of upper mantle composition from seismic velocity contrasts at 400 km depth, *Pure Appl. Geophys.*, *141*, 101–109, 1993.

Bina, C. R., and G. Helffrich, Phase transition Clapeyron slopes and transition zone seismic discontinuity topography, *J. Geophys. Res.*, *99*, 15,853–15,860, 1994.

Bina, C. R., and B. J. Wood, Olivine-spinel transitions: Experimental and thermodynamic constraints and implications for the nature of the 400-km seismic discontinuity, *J. Geopys. Res.*, *92*, 4853–4866, 1987.

Burnley, P. C., and H. W. Green, Stress dependence of the mechanism of the olivine-spinel transformation, *Nature*, *338*, 753–756, 1989.

Davies, G. F., and A. M. Dziewonski, Homogeneity and constitution of the Earth's lower mantle and outer core, *Phys. Earth Planet. Inter.*, *25*, 297–356, 1981.

Downs, R. T., C. S. Zha, T. S. Duffy, and L. W. Finger, The equation of state of forsterite to 17.2 GPa and effects of pressure media, *Am. Mineral.*, *81*, 51–55, 1996.

Duffy, T. S., and D. L. Anderson, Seismic velocities in mantle minerals and the mineralogy of the upper mantle, *J. Geophys. Res.*, *94*, 1895–1912, 1989.

Duffy, T. S., R. J. Hemley, and H. K. Mao, Equation of state and shear strength of MgO to 227 GPa, *Phys. Rev. Lett.*, *74*, 1371–1374, 1995a.

Duffy, T. S., C. S. Zha, R. T. Downs, H. K. Mao, and R. J. Hemley, Elasticity of forsterite to 16 GPa and the composition of the upper mantle, *Nature*, *378*, 170–173, 1995b.

Durbin, D. J., P. F. McMillan, and G. H. Wolf, Raman study of the high pressure behavior of forsterite (Mg_2SiO_4) crystal and glass, *Am. Mineral.*, *78*, 1143–1148, 1993.

Every, A. G., General closed-form expressions for acoustic waves in elastically anisotropic solids, *Phys. Rev. B*, *22*, 1746–1760, 1980.

Graham, E. K., and G. R. Barsch, Elastic constants of single-crystal forsterite as a function of temperature and pressure, *J. Geophys. Res.*, *74*, 5949–5959, 1969.

Gwanmesia, G. D., S. Rigden, I. Jackson, and R. C. Liebermann, Pressure dependence of elastic wave velocity for beta-Mg_2SiO_4 and the composition of the Earth's mantle, *Science*, *250*, 794–797, 1990.

Hazen, R. M., Effect of temperature and pressure on the crystal structure of forsterite, *Am. Mineral.*, *61*, 1280–1293, 1976.

Isaak, D. G., O. L. Anderson, T. Goto, and I. Suzuaki, Elasticity of single-crystal forsterite measured to 1700 K, *J. Geophys. Res.*, *94*, 5895–5906, 1989.

Ita, J., and L. Stixrude, Petrology, elasticity, and composition of the mantle transition zone, *J. Geophys. Res.*, *97*, 6849–6866, 1992.

Kudoh, Y., and Y. Takeuchi, The crystal structure of forsterite Mg_2SiO_4 under high pressure to 149 kbar, *Z. Kristallogr.*, *171*, 291–302, 1985.

Kumazawa, M., and O. L. Anderson, Elastic moduli, pressure derivatives, and temperature derivatives of single-crystal olivine and single-crystal forsterite, *J. Geophys. Res.*, *74*, 5961–5972, 1969.

Li, B., I. Jackson, T. Gasparik, and R. C. Liebermann, In situ elastic wave velocity measurements in multi-anvil apparatus to 10 GPa using ultrasonic interferometry, *Phys. Earth Planet. Inter.*, in press, 1996.

Mao, H. K., and P. M. Bell, Design and operation of a diamond-window high-pressure cell for the study of single-crystal samples loaded cryogenically, *Year Book Carnegie Inst. Washington*, *79*, 409–411, 1980.

Meade, C., and P. G. Silver, Laboratory and seismological observation of lower mantle isotropy, *Geophys. Res. Lett.*, *22*, 1293–1296, 1995.

Mock, R., B. Hillebrands, and J. R. Sandercock, Construction and performance of a Brillouin scattering set-up using a triple-pass tandem Fabry-Perot interferometer, *J. Phys. E*, *20*, 656–659, 1987.

Musgrave, M. J. P., *Crystal Acoustics*, Holden-Day, Merrifield, Va., 1970.

Nolet, G., S. P. Grand, and B. L. N. Kennett, Seismic heterogeneity in the upper mantle, *J. Geophys. Res.*, *99*, 23,753–23,766, 1994.

Olinger, B., Compression studies of forsterite (Mg_2SiO_4) and enstatite ($MgSiO_3$), in *High-Pressure Research: Applications in Geophysics*, edited by M. H. Manghnani and S. Akimoto, pp. 325–344, Academic, San Diego, Calif., 1977.

Poirier, J. P., On the kinetics of olivine-spinel transition, *Phys. Earth Planet. Inter.*, *26*, 179–187, 1981.

Press, W. H., S. A. Teukolsky, W. T. Vetterling, and B. P. Flannery, *Numerical Recipes in C*, Cambridge Univ. Press, New York, 1987.

Ringwood, A. E., *Composition and Petrology of the Earth's Mantle*, McGraw-Hill, New York, 1975.

Shimizu, H., and S. Sasaki, High-pressure Brillouin studies and elastic properties of single-crystal H_2S grown in a diamond cell, *Science*, *257*, 514–516, 1992.

Shimizu, H., W. A. Bassett, and E. M. Brody, Brillouin-scattering measurements of single-crystal forsterite to 40 kbar at room temperature, *J. Appl. Phys.*, *53*, 620–626, 1982.

Shimizu, H., M. Ohnishi, S. Sasaki and Y. Ishibashi, Cauchy relations in dense H_2O ice VII, *Phys. Rev. Lett.*, *74*, 2820–2823, 1995.

Watt, J. P., and L. Peselnick, Clarification of the Hashin-Shtrikman bounds on the effective elastic moduli of polycrystals with hexagnal, trigonal, and tetragonal symmetries, *J. Appl. Phys.*, *51*, 1525–1531, 1980.

Webb, S. L., The elasticity of the upper mantle orthosilicates olivine and garnet to 3 GPa, *Phys. Chem. Miner.*, *16*, 684–692, 1989.

Weidner, D. J., Elasticity of microcrystals, *Geophy. Res. Lett.*, *2*, 189–192, 1975.

Weidner, D. J., A mineral physics test of a pyrolite mantle, *Geophys. Res. Lett.*, *12*, 417–420, 1985.

Yoneda, A., and M. Morioka, Pressure derivatives of elastic constants of single crystal forsterite, in *High-Pressure Research: Applications to Earth and Planetary Sciences*, edited by Y. Syono and M. H. Manghnani, pp. 207–214, Terra Sci., Tokyo, 1992.

Zaug, J. M., E. H. Abramson, J. M. Brown, and L. J. Slutsky, Sound velocities in olivine at Earth mantle pressures, *Science*, *260*, 1487–1489, 1993.

Zha, C. S., T. S. Duffy, H. K. Mao, and R. J. Hemley, Elasticity of hydrogen to 24 GPa from single-crystal Brillouin scattering and synchrotron x-ray diffraction, *Phys. Rev. B*, *48*, 9246–9255, 1993.

Zha, C. S., R. J. Hemley, H. K. Mao, T. S. Duffy, and C. Meade, Acoustic velocities and refractive index of SiO_2 glass to 57.5 GPa by Brillouin scattering, *Phys. Rev. B*, *50*, 13,105–13,112, 1994.

T. S. Duffy, Consortium for Advanced Radiation Sources, University of Chicago, 5640 S. Ellis Avenue, Chicago, IL 60637.

R. T. Downs, R. J. Hemley, H.-K. Mao, C.-S. Zha, Geophysical Laboratory and Center for High-Pressure Research, Carnegie Institution of Washington, 5251 Broad Branch Road, N.W., Washington, DC 20015-1305.

(Received October 27, 1995; revised April 15, 1996;
accepted April 19, 1996.)